https://doi.org/10.2352/ISSN.2470-1173.2018.8.MAAP-166

Light Interreflections and Shadowing Effects in a Lambertian V-Cavity under Diffuse Illumination

Dorian Saint-Pierre[1], Rada Deeb[1], Damien Muselet[1], Lionel Simonot[1,2], Mathieu Hébert[1]; [1] Univ Lyon, UJM-Saint-Etienne, CNRS, Institut d'Optique Graduate School, Laboratoire Hubert Curien UMR 5516, F-42023, SAINT-ETIENNE, France, [2] Université de Poitiers, Institut Prime UPR CNRS 3346; Futuroscope Chasseneuil, France.

Abstract

The different areas of a concave object illuminate each other by a multiple light reflection process, called interreflections, depending on the geometries of the object and the lighting. For an accurate prediction of the radiance perceived from each point of the object by an observer or a camera, an interreflection model is necessary, taking into account the optical properties and the shape of the object, the orientation(s) of the incident light which can produce shadows, and the infinite number of light bounces between the different points of the object. The present paper focusses on the irradiance of two adjacent planar panels (V-cavity) illuminated by collimated light from any direction of the hemisphere, or by diffuse light. According to the reflectance of the material and the angle of the cavity, the loss of irradiance near the fold due to the shadowing effect is partly compensated by the gain in radiance due to the interreflections.

1. Introduction

Interreflection is an optical phenomenon occurring everywhere a concave surface is illuminated. It corresponds to the multiple reflections that light undergoes between the different areas of the surface, which result in a gain in radiance displayed by the surface at some wavelengths where the surface is weakly absorbing, therefore in a gain in lightness and/or chroma of their color, particularly noticeable in acute cavities. This is the case for example at the corner between two adjacent panels illuminated frontally by directional light, shown in Figure 1. This phenomenon has gained a lot of attention in computer graphics in order to improve the rendering quality of scenes where various objects exchange light between each other (typically a colored object close to a white wall) [1–3]. It has also been studied in the domain of computer vision, in order to remove this effect from images of an object in order to retrieve the object's 3D shape (shape-from-shading methods) [4–9] or its spectral reflectance as well as the illuminant spectral power distribution [10–11].

In most previous studies, interreflections are modeled by considering only two or three bounces of lights, but we can show that in the case of Lambertian surfaces with high reflectance, at least in a given part of the visible spectrum, it is necessary to take into account all successive bounces until infinity in order to obtain an accurate prediction of the luminances displayed by the object.

The gain in lightness and chroma characteristic of interreflections illustrated by Figure 1 is well visible when the incident light is rather directional and illuminates the whole surface. However, in case of oblique lighting, the concavities may be only partly illuminated because of shadowing. Moreover, in case of diffuse lighting the shadowing effect diminishes the irradiance of the surface in the concavities, and the aforementioned visual effects consequently vanishes. The picture in Figure 2 shows that under a perfectly diffuse lighting, a folded piece of board is darker near the fold, whereas it would appear lighter under collimated illumination as in Figure 1. The main question resulting from this observation is to know to which extent interreflections, which increase the perceived radiance in the concavities of the surface, compensates shadowing, which decreases the irradiance, according to the shape of the surface, its reflectance, and the illumination geometry.

Throughout this paper, we will consider the simple case of a V-cavity, similar to the folded pieces of board shown in Figures 1 and 2, but with infinite length (along the fold). This allows interesting analytical solutions for the interreflection model that we will use, which takes into account an infinity of light bounds. After a Section 2 dedicated to terms and notations, this interreflection

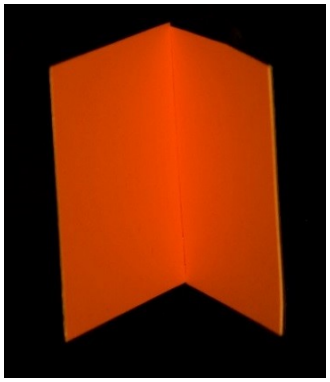

Figure 1 – Picture made with a RGB camera of a V-cavity with an angle of 45° between the two panels (folded Lambertian Munsell paper) illuminated frontally by collimated light. The color gradient visible near the fold is due to the interreflection effect.

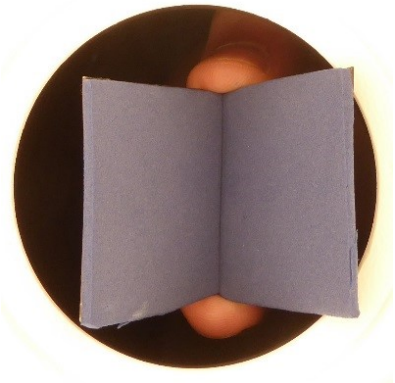

Figure 2 – V-cavity with an angle of 45° between the two panels made of a grey Lambertian material, illuminated by perfectly diffused light in an integrating sphere.

model is presented in Section 3, in the general case of a 3D-shaped Lambertian material, then in the special case of a V-cavity of infinite length. We then address the question of the illumination geometries and the shadowing model in Section 4, before studying their influence on the displayed radiance in Section 5. Finally, Section 6 draws the conclusions.

2. Definitions and notations

The description of the interreflection effect is based on radiometric concepts allowing to describe how light is spatially distributed in the scene. The light power, or flux, denoted as F, can be regarded as a collection of light rays propagating from the source to the objects, then from areas of the objects to other areas, then from the objects to the observer. The distribution of the light power over a given surface is described by the concept of *irradiance* (for incoming light) or *exitance* (for outgoing light), defined as the density of flux per elemental area dA:

$$E = \frac{dF}{dA} \tag{1}$$

Radiance, denoted as L, is defined by the density of light power (or flux) d^2F per elemental geometrical extent d^2G:

$$L = \frac{d^2F}{d^2G} \tag{2}$$

where the geometrical extent describes the flux transfer volume, as featured in Figure 3. By denoting respectively as dP_i and dP_j the elemental areas located around two points P_i and P_j distant by a length Δ, we can define d^2G as:

$$d^2G(P_i,P_j) = \frac{dP_i \cos\theta_i dP_j \cos\theta_j}{\Delta^2} \tag{3}$$

where θ_i and θ_j are the angles between the line (P_iP_j) and the normal of the elemental areas dP_i and dP_j, respectively.

The irradiance in point P_i is denoted as $E(P_i)$, and the radiance from point P_i to point P_j is denoted as $L(P_i,P_j)$.

A surface able to reflect similar radiance in every direction (therefore towards any point in the scene) is called a Lambertian surface. In this case, the radiance issued from P_i in any direction is a constant, simply denoted as $L(P_i)$. According to Lambert's law,

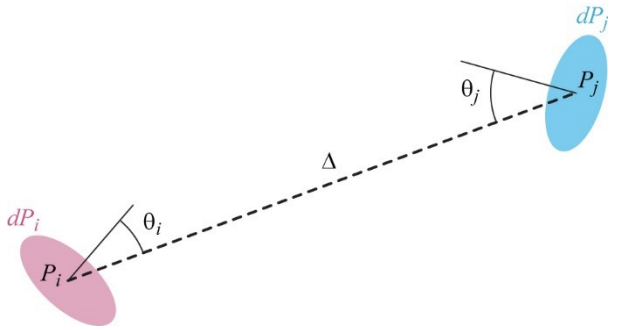

Figure 3 – Geometrical extent subtended by elemental areas around two points P_i and P_j

it is proportional to the surface reflectance r_i and the irradiance $E(P_i)$ in P_i:

$$L(P_i) = \frac{r_i}{\pi} E(P_i) \tag{4}$$

The direct irradiance received in a point P_i from the light source and the radiance after the first light reflection of the surface are denoted respectively as E_0 and L_1. This direct irradiance E_0, the radiance L and the radiance after one reflection, L_1, can also be defined for a collection of small areas on the surface (e.g. corresponding to a tessellation of the surface), and are in this case represented under the form of vectors:

$$\begin{aligned} \mathbf{E_0} &= \begin{bmatrix} E_0(P_1) & E_0(P_2) & \cdots \end{bmatrix} \\ \mathbf{L} &= \begin{bmatrix} L(P_1) & L(P_2) & \cdots \end{bmatrix} \end{aligned} \tag{5}$$

where the superscript T denotes the transpose operator.

Notice that all radiometric quantities are wavelength-dependent. Throughout this paper, in order to shorten the notation, we will consider these quantities for one wavelength which can be any wavelength of the visible spectrum.

3. Radiometric model for interreflections

Modelling interreflections of light in a concave surface means modelling the multiple bounds of photons between the different areas of the surface before reaching the observer. After having introduced a generic interreflection model applicable to any 3D-shaped Lambertian surface, we will show how this generic model is implemented in the special case of a V-cavity of infinite length.

General case

One way of writing the observed radiance from a 3D-shaped Lambertian surface S, by taking into account the contribution of the multiple light bounces between each pair of points P_i and P_j on the surface, is based on a continuous equation known as the radiosity equation, or interreflection equation [12-**Error! Reference source not found.**], which expresses the total radiance $L(P_i)$ perceived from every point P_i as the sum of two terms: 1) the radiance $L_1(P_i)$ after one bounce, corresponding to the observed photons issued from the light source of irradiance $E_0(P_i)$ and reflected once on the surface of reflectance r_i in P_i:

$$L_1(P_i) = \frac{r_i}{\pi} E_0(P_i) \tag{6}$$

and 2) the radiance after multiple bounces, corresponding to the observed photons issued from every other point P_j of the surface and reflected one more time on the surface in P_i. Each point P_i emits the radiance $L(P_j)$ in every direction, therefore towards point P_i, and the elemental irradiance received in P_i from P_j is

$$K(P_i,P_j) L(P_j) dP_j$$

where $K(P_i,P_j)$ is a function called geometrical kernel (or interreflection kernel) related to the geometrical extent subtended

by points P_i and P_j on the surface, defined by equation (3):

$$K\left(P_i,\,P_j\right)=\frac{d^2G\left(P_i,P_j\right)}{dP_i dP_j}V\left(P_i,P_j\right), \tag{7}$$

$V\left(P_i,P_j\right)$ being a visibility function that gives 1 when both elementary areas dP_i and dP_j can see each other, and 0 otherwise. The radiance after multiple bounces, which incorporates the elemental irradiances in P_i formed by the light coming from all other points P_j of the surface S, is therefore

$$\frac{r_i}{\pi}\int_{P_j\in S}K\left(P_i,P_j\right)L\left(P_j\right)dP_j$$

and the total radiance $L\left(P_i\right)$ displayed by point P_i is given by:

$$L\left(P_i\right)=\frac{r_i}{\pi}\left[E_0\left(P_i\right)+\int_{P_j\in S}K\left(P_i,P_j\right)L\left(P_j\right)dP_j\right] \tag{8}$$

The integral equation (8) has no analytical solution in the general case. It can be solved numerically or, more conveniently, converted into a discrete version after sampling the surface, thus represented by a collection of n microfacets having same area, as proposed by Nayar *et al.* [4**Error! Reference source not found.**].

By considering both radiance and reflectance constant over each facet, represented by a point P_i and its finished area ΔP_i, the integral equation (8) becomes:

$$L(P_i)=\frac{r_i}{\pi}\left[E_0(P_i)+\sum_{j\neq i}K_{ij}L(P_j)\right] \tag{9}$$

where

$$K_{ij}=\int_{P\in\Delta P_j}K(P_i,P)dP \tag{10}$$

This allows transforming the geometrical kernel into a matrix

$$\mathbf{K}=\begin{pmatrix}0 & K_{12} & \cdots & \\ K_{21} & 0 & \cdots & \\ \vdots & \vdots & \ddots & \vdots \\ K_{n1} & K_{n2} & \cdots & \end{pmatrix} \tag{11}$$

which is symmetrical as $K_{ij} = K_{ji}$ for every i and j.

Since each facet has its proper spectral reflectance, we gather all facet's reflectances into an $n \times n$ diagonal matrix whose ith entry on the diagonal is the reflectance of facet i:

$$\mathbf{R}=\begin{pmatrix}r_1 & 0 & \cdots & \\ 0 & r_2 & & \vdots \\ \vdots & & \ddots & \\ 0 & \cdots & & r_n\end{pmatrix} \tag{12}$$

We can finally write Eq. (9) as:

$$\mathbf{L}=\frac{1}{\pi}\mathbf{R}\left[\mathbf{E_0}+\mathbf{KL}\right] \tag{13}$$

where vectors $\mathbf{L}$ and $\mathbf{E_0}$ are defined in Eq. (5), or equivalently as:

$$\mathbf{L}=\frac{1}{\pi}\left(\mathbf{I}-\frac{1}{\pi}\mathbf{RK}\right)^{-1}\mathbf{RE_0} \tag{14}$$

where $\mathbf{I}$ is the $n \times n$ identity matrix. All terms contained in this general matrix equation are wavelength-dependent. The equation is therefore written for each wavelength of light.

Remark: the computation of the terms K_{ij} defined by equation (10) needs an important comment. When points P_i and P_j are far from each other, we can assume that function $K(P_i,P_j)$ is nearly constant over the integration domain and therefore that equation (10) can be simplified as

$$K_{ij}\approx K(P_i,P_j)\Delta P_j \tag{15}$$

However, this approximation is not valid for adjacent facets, i.e., when P_i and P_j are close to each other. In this case, K_{ij} must be computed by integration as defined in equation (10), either analytically when possible, or numerically.

Special case of a V-cavity of infinite length

In the present study, we consider the interreflections in a "V-cavity" drawn by two adjacent planar panels forming an angle α, as shown in Figure 4. The two panels will be labelled 1 and 2. The common edge of the panels, assumed to be of infinite length, defines the x-axis of the 3D Cartesian space. The width of both panels is set to unity (it could be equivalently any other value: the width has no impact on the interreflection effect in this configuration as we will show later). The y- and z-axes belong to the plane orthogonal to the x-axis, the z-axis being in the bisector plane between the two panels. Hence, each panel forms an angle α/2 with the z-axis. Moreover, the position of points in the panels will be described by proper bi-dimensional coordinate systems: (x,y') in panel 1 and (x,y'') in panel 2, where the y' and y'' axes belong respectively to panel 1 and panel 2 and are perpendicular to the x axis. Since the V-cavities considered in this paper have an infinite length according to the x-axis, their geometry depends only on angle α.

The general interreflection equation (14), in particular the

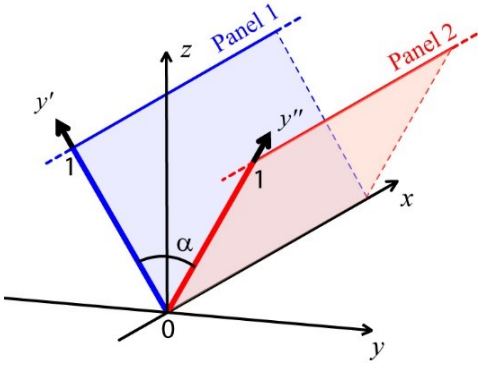

Figure 4 – 3D Geometry of a V-cavity.

matrices **R** and **K**, can be adapted to the V-cavity of infinite length made of a uniform Lambertian material as follows.

Regarding matrix **R**, since the two panels are uniform and made of the same Lambertian material, all facets have the same reflectance *r*. Hence, matrix **R** is a diagonal matrix where all terms on the diagonal are *r*, and can therefore be replaced with *r***I**, where **I** is the $2p \times 2p$ unity matrix. Eq. (14) can therefore be written as:

$$\mathbf{L} = \frac{r}{\pi}\left(\mathbf{I} - \frac{r}{\pi}\mathbf{K}\right)^{-1}\mathbf{E_0} \tag{16}$$

Regarding matrix **K**, it is built according to a tessellation of the panels into $2p$ facets, and has therefore the dimension $2p \times 2p$. Each of the two panels is decomposed into p facets of infinite length (according to the x-axis) and finite width (according to the y' or y'' axis, accordingly). Since the total width of each panel is unity, the width of each facet is $1/p$. The entries K_{ij} of matrix **K** are computed according to Eq. (10), where function $K(P_i,P_j)$ is defined by Eq. (7). The visibility function $V\left(P_i,P_j\right)$ introduced in equation (7) is 0 for facets belonging to the same panel, and 1 for facets belonging to different panels. The geometrical extent $d^2G\left(P_i,P_j\right)$, also introduced in equation (7), must take into account the fact that we have here facets of infinite length. It has an analytical expression that we propose to derive now.

Let us consider on panel 1 a point P_i of coordinates $\left(x_i,y_i'\right)$ in the (x, y')-coordinate system used for panel 1, and a point P_j of coordinates $\left(x_j,y_j''\right)$ in the (x, y'')-coordinate system used for panel 2, as featured in Figure 5. We also consider on panel 2 a facet of infinite length whose edges are parallel to the x-axis. Its highest edge meets point P_j at the ordinate y_j'' and, since every facet has a width $1/p$, its lower edge is at the ordinate $y_j''-1/p$. We want to express first the geometrical extent subtended by elemental areas dP_i and dP_j around points P_i and P_j, then the geometrical extent subtended by dP_i and the whole facet j.

In the 3D Cartesian system introduced in Figure 4, the points P_i and P_j have the coordinates

$$P_i = \begin{pmatrix} x_i \\ -y_i'\sin(\alpha/2) \\ y_i'\cos(\alpha/2) \end{pmatrix} \quad \text{and} \quad P_j = \begin{pmatrix} x_j \\ y_j''\sin(\alpha/2) \\ y_j''\cos(\alpha/2) \end{pmatrix} \tag{17}$$

and the normal of dP_i and dP_j, corresponding to the normals $\mathbf{N_1}$ and $\mathbf{N_2}$ of panels 1 and 2, respectively, are:

$$\mathbf{N_1} = \begin{pmatrix} 0 \\ \cos(\alpha/2) \\ \sin(\alpha/2) \end{pmatrix} \quad \text{and} \quad \mathbf{N}_2 = \begin{pmatrix} 0 \\ -\cos(\alpha/2) \\ \sin(\alpha/2) \end{pmatrix} \tag{18}$$

The angles θ_i and θ_j formed by the line $\left(P_iP_j\right)$ and the normals $\mathbf{N_1}$, respectively $\mathbf{N_2}$, therefore satisfy the equations:

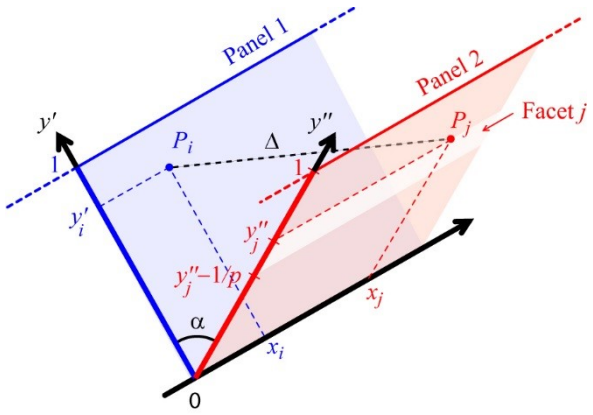

Figure 5 – Geometrical configuration where a point P_i on panel 1 sees a facet of infinite length on panel 2.

$$\cos\theta_i = \frac{1}{\Delta}\begin{pmatrix} x_j - x_i \\ y_j''\sin(\alpha/2) + y_i'\sin(\alpha/2) \\ y_j''\cos(\alpha/2) - y_i'\cos(\alpha/2) \end{pmatrix} \cdot \begin{pmatrix} 0 \\ \cos(\alpha/2) \\ \sin(\alpha/2) \end{pmatrix}$$

and

$$\cos\theta_j = \frac{1}{\Delta}\begin{pmatrix} x_i - x_j \\ -y_i'\sin(\alpha/2) - y_j''\sin(\alpha/2) \\ y_i'\cos(\alpha/2) - y_j''\cos(\alpha/2) \end{pmatrix} \cdot \begin{pmatrix} 0 \\ -\cos(\alpha/2) \\ \sin(\alpha/2) \end{pmatrix}$$

where symbol · denotes the dot product between vectors, and Δ denotes the length P_iP_j:

$$\begin{aligned} \Delta &= \sqrt{\left(x_i - x_j\right)^2 + \left(y_i' + y_j''\right)^2\sin^2\left(\tfrac{\alpha}{2}\right) + \left(y_i' - y_j''\right)^2\cos^2\left(\tfrac{\alpha}{2}\right)} \\ &= \sqrt{\left(x_i - x_j\right)^2 + y_i'^2 + y_j''^2 - 2y_i'y_j''\cos\alpha} \end{aligned} \tag{19}$$

After computation, one obtains:

$$\cos\theta_i = \frac{y_j''\sin\alpha}{\Delta} \quad \text{and} \quad \cos\theta_j = \frac{y_i'\sin\alpha}{\Delta} \tag{20}$$

The elemental area dP_i around P_i can be written dx_idy_i' and the elemental area dP_j around P_j, dx_jdy_j''.

Finally, according to Eqs. (3), (19) and (20), the geometrical extent is written:

$$d^4G = \frac{y_i'y_j''\sin^2\alpha}{\left[\left(x_i - x_j\right)^2 + y_i'^2 + y_j''^2 - 2y_i'y_j''\cos\alpha\right]^2}dx_idy_i'dx_jdy_j'' \tag{21}$$

and the interreflection Kernel defined by Eq. (7) becomes

$$K\left(x_i,y_i',x_j,y_j''\right) = \frac{y_i'y_j''\sin^2\alpha}{\left[\left(x_i - x_j\right)^2 + y_i'^2 + y_j''^2 - 2y_i'y_j''\cos\alpha\right]^2} \tag{22}$$

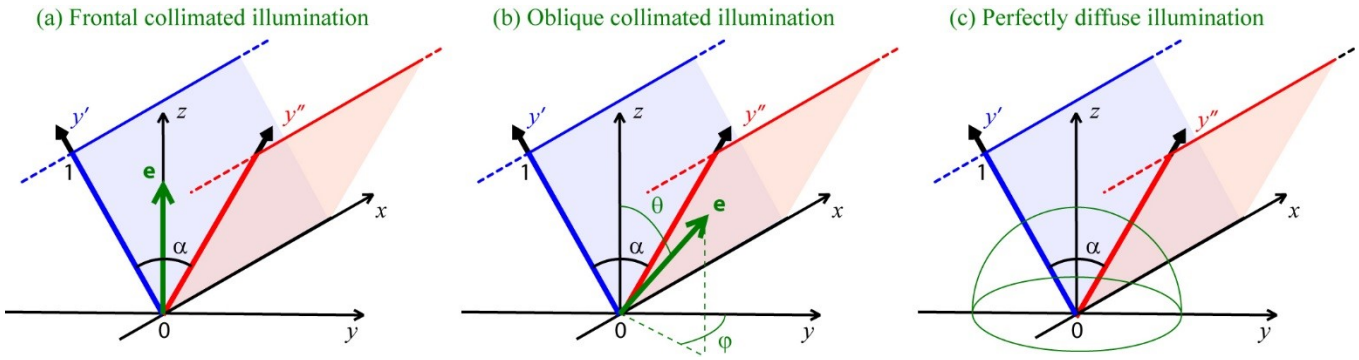

Figure 6 - Geometry of the V-cavity and the considered illuminations.

Regarding the non-zero entries of matrix **K**, defined by Eq. (10) in the case where P_i and P_j belong to different panels, they are obtained by integrating the interreflection Kernel $K(x_i, y_i', x_j, y_j'')$, given by Eq. (22), over the facet, i.e., between $-\infty$ to ∞ along the *x*-axis, and between $y_j'' - 1/p$ and y_j'' along the y''-axis:

$$K_{ij} = \int_{x=-\infty}^{\infty} \int_{y''=y_j''-1/p}^{y_j''} \frac{y_i' y'' \sin^2\alpha \, dx dy''}{\left[(x_i - x)^2 + y_i'^2 + y''^2 - 2 y_i' y'' \cos\alpha\right]^2} \qquad (23)$$

This double integral has an analytical solution, given by:

$$K_{ij} = F(y_j'') - F\left(y_j'' - \tfrac{1}{p}\right) \qquad (24)$$

with

$$F(u) = \frac{\pi}{2} \frac{u\cos\alpha - y_i'}{\sqrt{y_i'^2 + u^2 - 2 y_i' u \cos\alpha}}$$

Unsurprisingly, K_{ij} is independent of x_i. This is due to the infinite length of the V-cavity which generates an invariant interreflections process along the *x* axis.

Finally, matrix **K** in Eq. (16) is a $2p \times 2p$ matrix whose entries are 0 for pairs of facets belonging to the same panel, and are given by Eq. (24) for pairs of facets belonging to different panels, knowing that $K_{ij} = K_{ji}$.

4. Illumination Geometries

In the radiance equation (16), the term $\mathbf{E_0}$ denotes the direct irradiance of the different facets in the V-cavity (without taking into account the interreflections), which depends on the geometrical configuration of illumination. In this study, we consider that the lighting is uniform and covers the whole V-cavity. Three configurations are considered, featured in Figure 6: frontal directional lighting, where the incoming light is parallel to the *z*-axis; oblique directional lighting where the incoming light is parallel to a vector **e**, featured in Figure 5 by a green arrow, forming a polar angle θ in respect to the *z*-axis and an azimuthal angle φ in respect to the (*y*, *z*)-plane; and perfectly diffuse lighting, characterized by a radiance uniformly distributed over the hemisphere. In every case, the lighting covers uniformly the whole cavity area. The aim of this section is to study the influence of the angular distribution of incident light on the radiance displayed by the cavity in each point by taking into account to possible shadows that one panel may project onto the other panel.

Directional Lighting

We first consider a frontal collimated lighting, parallel to the *z*-axis, i.e., $\mathbf{e} = [0 \quad 0 \quad 1]^T$. The horizontal plane (*x*, *y*) receives an irradiance denoted as E_z. It is the maximum direct irradiance that a panel can receive. Under this frontal illumination, since both panels form an angle α/2 with the vector **e**, each one receives an irradiance $E_z \sin(\alpha/2)$. All entries of vector $\mathbf{E_0}$ are therefore identical:

$$\mathbf{E_0} = E_z \sin\left(\tfrac{\alpha}{2}\right)[1 \quad \cdots \qquad (25)$$

Under an oblique illumination, where the collimated light is parallel to the vector

$$\mathbf{e} = (\sin\theta\sin\varphi \quad \sin\theta\cos\varphi \quad \cos\theta)^T, \qquad (26)$$

the panels receive an irradiance given by

$$E_z \langle \mathbf{e} \cdot \mathbf{N}_i \rangle \qquad (27)$$

where the symbol $\langle \cdot \rangle$ denotes the clamped dot product between the illumination vector **e** and the normal $\mathbf{N}_i$ of the panel $i = 1$ or 2, given by Eq. (18), or equal to 0 when the dot product is negative since the surface is not illuminated when the angle between the incident light direction and the surface normal exceeds 90°.

Hence, for an oblique illumination, the entries of vector $\mathbf{E_0}$ are $E_z\left[u\sin\theta\cos\varphi\cos(\alpha/2) + \cos\theta\sin(\alpha/2)\right]$ with $u = 1$ for the *p* first entries attached to the facets on panel 1, and $u = -1$ for the *p* last entries attached to the facets on panel 2.

Moreover, part of a panel may also be not illuminated because of shadowing by the other panel. Shadowing can be taken into account into the interreflection equation (16) by simply setting to 0 the entries of the irradiance vector $\mathbf{E_0}$ corresponding to the non-illuminated facets, thanks to a diagonal matrix $\mathbf{S_h}$ of size $2p \times 2p$ whose *j*th entry on the diagonal is 1 if the *j*th facet is illuminated, and 0 otherwise. The interreflection equation modified as follows automatically takes into account the fact that some facets may be

not directly illuminated by the light source:

$$\mathbf{L} = \frac{r}{\pi}\left(\mathbf{I} - \frac{r}{\pi}\mathbf{K}\right)^{-1} \mathbf{S_h E_0} \tag{28}$$

The Boolean values in this diagonal matrix $\mathbf{S_h}$ are given by a function $S_j(\theta,\varphi)$ depending on the orientation of illumination, computed according to a condition that the central point F of each facet j of the V-cavity satisfies or not, and that we propose to introduce now.

First of all, we can observe that shadowing does not occur if vector **e** is parallel to the (x, z) plane. It occurs only if the vector $\mathbf{e}^{\perp}$ obtained by projection of vector **e** onto the (y, z) plane forms an angle larger than α/2. This projected vector $\mathbf{e}^{\perp}$ can be defined by its coordinates (y_e, z_e) in the (y, z) plane:

$$\mathbf{e}^{\perp} = \begin{pmatrix} y_e \\ z_e \end{pmatrix} = \begin{pmatrix} \sin\theta\cos\varphi \\ \cos\theta \end{pmatrix} \tag{29}$$

In Figure 7, the projections of panels 1 and 2 onto the (y, z) plane are represented by a blue segment OA and a red segment OB, respectively. Vector $\mathbf{e}^{\perp}$, represented by a green arrow, is based on the central point F of a facet located on panel 1, at a distance y'_F from the fold (point O):

$$\mathrm{F} = \begin{pmatrix} y_F \\ z_F \end{pmatrix} = \begin{pmatrix} -y'_F \sin(\alpha/2) \\ y'_F \cos(\alpha/2) \end{pmatrix} \tag{30}$$

The line parallel to vector $\mathbf{e}^{\perp}$ that meets point F intersects line (AB) in a point G whose coordinates in the (y, z) plane satisfy both line equations:

$$\begin{aligned} &(\mathrm{AB}): \quad z_G = \cos\left(\tfrac{\alpha}{2}\right) \\ &(\mathrm{FG}): \quad z_G = z_F + (y_G - y_F)\frac{z_e}{y_e} \end{aligned} \tag{31}$$

By solving this system of two equations, one obtains:

$$y_G = (1 - y'_F)\tan\theta\cos\varphi\cos\left(\tfrac{\alpha}{2}\right) - y'_F \sin\left(\tfrac{\alpha}{2}\right) \tag{32}$$

The condition for this point F on panel 1 to be illuminated is that G is between A and B, i.e., that $|y_G| < \sin(\alpha/2)$, which yields the condition:

$$\left|(1 - y'_F)\tan\theta\cos\varphi\cos\left(\tfrac{\alpha}{2}\right) - y'_F \sin\left(\tfrac{\alpha}{2}\right)\right| < \sin\left(\tfrac{\alpha}{2}\right) \tag{33}$$

The Boolean function $S_i(\theta,\varphi)$ used to determine the values of the first p entries on the diagonal of matrix $\mathbf{S_h}$ is 1 is the central point F of the ith facet satisfies the inequality (33), and 0 otherwise.

Similar reasoning line applies when the point F is on panel 2, except that its coordinates in the (y, z) plane are:

$$\mathrm{F} = \begin{pmatrix} y_F \\ z_F \end{pmatrix} = \begin{pmatrix} y''_F \sin(\alpha/2) \\ y''_F \cos(\alpha/2) \end{pmatrix}$$

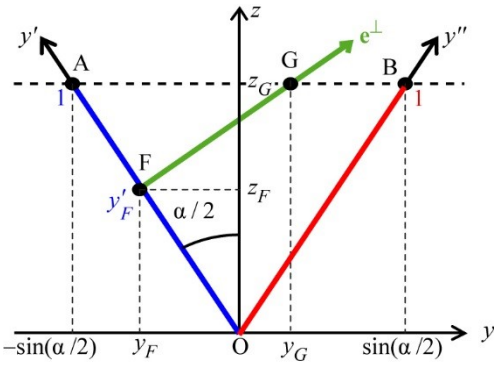

Figure 7 – Geometry of the V-cavity and the illumination vector projected onto the plan (y, z) plane.

and the inequality of Eq. (33) becomes

$$\left|(1 - y''_F)\tan\theta\cos\varphi\cos\left(\tfrac{\alpha}{2}\right) + y''_F \sin\left(\tfrac{\alpha}{2}\right)\right| < \sin\left(\tfrac{\alpha}{2}\right) \tag{34}$$

The Boolean function $S_j(\theta,\varphi)$ used to determine the values of the last p entries on the diagonal of matrix $\mathbf{S_h}$ is 1 if the central point F of the $p+j$th facet satisfies the inequality (34), and 0 otherwise.

Diffuse lighting

Another type of lighting geometry is the perfectly diffuse light, also called Lambertian illumination (see Figure 5.c). Under this lighting, a horizontal plan would receive same radiance L_0 from every direction of the hemisphere, forming on the (x, y) plane a total irradiance E_z related to L_0 by:

$$E_z = \int_{\varphi=0}^{2\pi}\int_{\theta=0}^{\pi/2} L_0 \cos\theta\sin\theta d\theta d\varphi = \pi L_0 \tag{35}$$

In the case of the V-cavity, because of the shadowing effect, the panels are not homogeneously illuminated: the points near the edges are more illuminated than the ones near the fold. The irradiance $E_{0,j}$ on each facet j of the V-cavity can be computed thanks to the Boolean function $S_j(\theta,\varphi)$ introduced previously:

$$E_{0,j} = \int_{\varphi=0}^{2\pi}\int_{\theta=0}^{\pi/2} L_0 S_j(\theta,\varphi)\cos\theta\sin\theta d\theta d\varphi \tag{36}$$

The entries of the vector $\mathbf{E_0}$ are computed according to this equation (36), and the interreflection equation (16) can be used to predict the radiance observed from the facets of the cavity.

Figure 8 shows the irradiance distribution on panel 1 along the y'-axis, for various cavities characterized by different angles α between the panels, all illuminated by a Lambertian lighting that produces an irradiance unity $(E_z = 1)$ on a horizontal flat surface (α = 180°). Similar distribution would be observed on panel 2 along the y''-axis. It is interesting to observe that the irradiance

received by the panel is lower near the fold than near their external edges. As α decreases, the irradiance is decreased by a factor $\sin(\alpha/2)$ in every position y' [see Eq. (25)], and is even more decreased as y' tends to zero due to the shadowing effect.

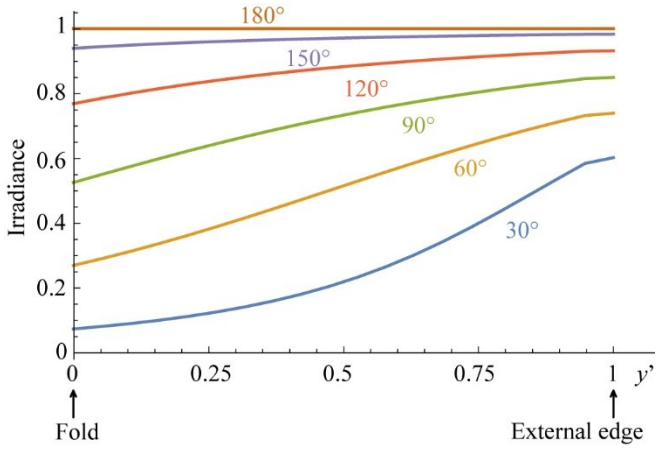

Figure 8 – Direct irradiance on panel 1 along the y' axis, from 0 (fold) to 1 (external edge), for a panel of V-cavities characterized by different angles α under a Lambertian illumination producing an irradiance E_z = 1 on the horizontal plane.

The first simulation is based on a V-cavity whose panels form an angle α = 45°, made of a Lambertian material with spectral reflectance $r(\lambda)$ corresponding to a magenta color. The V-cavity is illuminated by collimated light, parallel to the z-axis (frontal

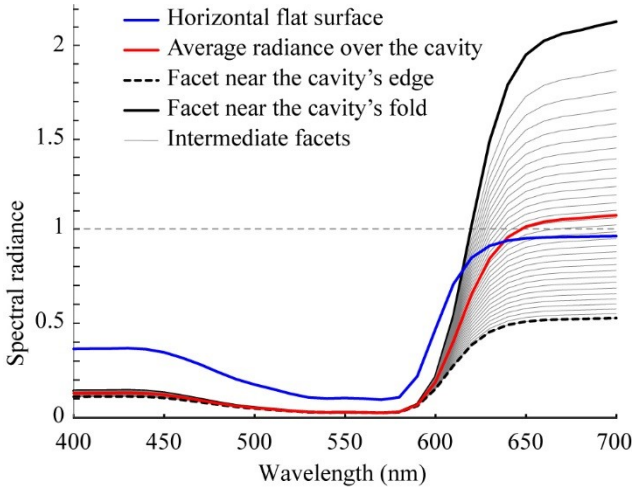

Figure 9 – Simulated spectral radiances perceived from a flat Lambertian surface of magenta material illuminated by frontal collimated irradiance E_z = π, and from facets of a V-cavity of angle α = 45° under similar irradiance.

Other illumination geometries

More complex illumination geometries can be considered as soon as the radiance $L_0(\theta,\varphi)$ coming from every direction of the hemisphere is known. The entries of vector $\mathbf{E}_0$ are thus computed according to the following equation, which extends Eq. (36):

$$E_{0,j} = \int_{\varphi=0}^{2\pi}\int_{\theta=0}^{\pi/2} L_0(\theta,\varphi) S_j(\theta,\varphi)\cos\theta\sin\theta d\theta d\varphi \qquad (37)$$

Outdoor lighting in a sunny day can often be modeled as the sum of direct illumination from the sun and diffuse illumination from the blue sky that we can consider as Lambertian in a first approximation. In this case, two vectors $\mathbf{E}_{0,direct}$ and $\mathbf{E}_{0,diffuse}$ can be computed for the sunlight according to the orientation of the sun, respectively for the diffuse light from the sky, by reminding that two spectral power distribution of the two lightings are different. The global irradiance vector $\mathbf{E}_{0,direct}$ is a linear combination of the two vectors

$$\mathbf{E}_{\mathbf{general}} = (1-b)\mathbf{E}_{0,direct} + b\mathbf{E}_{0,diffuse} \qquad (38)$$

with b a real number between 0 and 1.

5. Perceived radiance according to the illumination geometry

The present section aims at using the interreflection model introduced in the previous sections to study, through various simulations, the influence of the illumination geometry on the gradient of radiances displayed by the V-cavity, as well as the one of the surface reflectance.

Collimated lighting

illumination), producing an irradiance $E_z = \pi$ on a horizontal plane parallel to the (x, y) plane. Under this illumination, the radiance displayed by a perflectly white (reflectance $r = 1$), lambertian, flat and horizontal surface would be $L = E_z/\pi = 1$. The cavity is observed frontally, along the z-axis. The radiance displayed by similar surface but with a spectral reflectance $r(\lambda)$ corresponding to a magenta color is plotted with a blue line in Figure 9. We also consider a V-cavity made of this magenta material whose panels form an angle α = 45°. Due to the obliqueness of the panels, their irradiance is $E_z \sin(\alpha/2)$, which represents only 39% of the irradiance E_z on the horizontal flat surface. The spectral radiances displayed by the different facets of panel 1, given by Eq. (28), are plotted in Figure 9 in grey lines except the ones issued from the two facets located near the fold $(y' \to 0)$ and near the external edge $(y' \to 1)$, which are plotted in solid black line and dashed black line, respectively. Notice that similar spectral radiances are displayed by panels 1 and 2 under this frontal lighting.

Near the external edge of the cavity, the interreflection effect is weak: the perceived radiance in this area (plotted with a dashed line) is made of photons having undergone at most one or two bounces on the panels and its spectral distribution is close to the one of the radiance displayed by the flat horizontal surface (plotted with a blue line), on which photons undergo one bounce only. The difference between these two spectra relies mainly on the wavelength- independent irradiance factor $\sin(\alpha/2)$ due to the oblique illumination of the panel. In contrast, the interreflection effect is strong near the fold: the radiance displayed in these areas is higher, especially in the spectral domain for which the material is highly reflecting (reflectance r higher than 0.7): the radiance noticeably overpasses the one displayed by the flat surface. The

color of the panels is clearly more saturated near the fold than near the edges, as shown in Figure 1.

The average radiance that would be observed far from the cavity, plotted with a red line, is darker that the one issued from the flat surface in the spectral domain where the material is the more absorbing (i.e., the less reflecting), but it is lighter in the rest of the spectrum. The average color of the V-cavity is more saturated than the one of the flat surface.

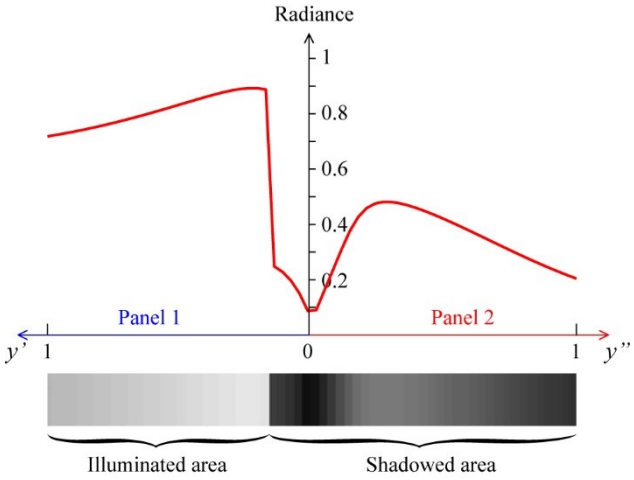

Figure 10 – Simulated spectral radiance perceived from the two panels of a V-cavity of angle α = 45° and reflectance r = 1, illuminated by oblique collimated irradiance $E_z = \pi$ coming from the direction (θ, φ) = (30°, 0°). A slice of the cavity, perpendicular to the x-axis, is shown in grey level below the graph.

We also simulated the radiance exhibited by this cavity when illuminated with oblique collimated light in a configuration where shadowing occurs. The incidence direction forms an angle of 30° with the z-axis, and is parallel to the (y, z) plane. Panel 1 is only partly illuminated, and panel 2 is not illuminated at all. The radiance profile displayed by the two panels, along the y'- and y''-axes, is plotted and shown under the form of a grey level image in Figure 10. We can see that even though panel 2 is not directly illuminated, it is illuminated by interreflections with panel 1 and displays a non-zero radiance.

Diffuse lighting

After the simulations done for collimated light, we performed simulations for a Lambertian illumination by considering same material, same cavity geometry, and same irradiance $E_z = \pi$ on the flat surface as for the frontal collimated lighting. Observation is still frontal, along the z-axis. The radiances displayed by the different facets of panel 1 along the y'-axis are plotted in Figure 11, by using the same line style as in Figure 9. The radiances displayed by panel 2 are similar. We observe that the facets near the external edge receive a higher irradiance under this Lambertian lighting (76% of the irradiance E_z on the horizontal surface) than under frontal collimated lighting (39%). The spectral radiances displayed in these areas where the interreflection effect is the weakest are therefore higher in Figure 11 than in Figure 9 (see dashed lines), but remain lower than the one issued from the flat surface (blue line). Near the fold where the interreflections are the strongest, the irradiance is strongly decreased by the shadowing effect. The facets in this area display a lower radiance (solid black line) than the ones near the external edge (dashed black line), despite the effect of the interreflections. This is visible in Figure 2 through the picture of a V-cavity made of grey Lambertian material, placed into an integrating sphere which provides the Lambertian illumination.

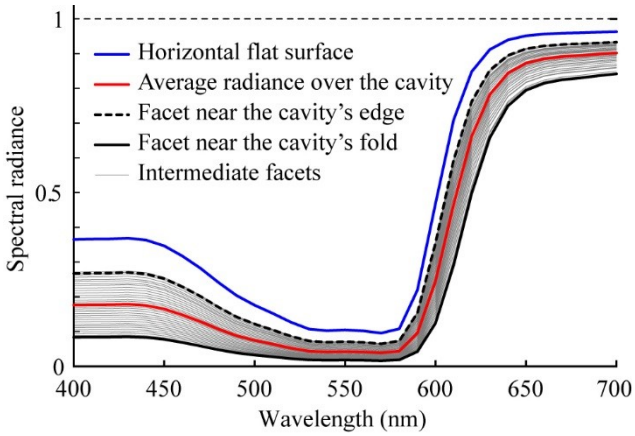

Figure 11 – Simulated spectral radiances perceived from a flat Lambertian surface of magenta material illuminated by a Lambertian irradiance $E_z = \pi$, and from facets of a V-cavity of angle α = 45° under similar irradiance.

There is therefore a competition between the interreflection effect, which tends to increase the radiance, and the shadowing effect, which tends to decrease it. This latter is clearly the strongest in the case of a Lambertian illumination, but we wanted to investigate the case of other illumination geometries for which the competition between the two effects could be more equitable, in particular the case of mixed collimated and diffuse illuminations.

Mixing direct and diffuse lightings

The variation of perceived radiance on panel 1 of a cavity of angle α = 45°, along the y'-axis from the fold (y' = 0) to the external edge (y' = 1), have been simulated by using the interreflection model and plotted in Figure 12 for two values of the material's reflectance, r = 1 and r = 0.8, and various illumination geometries combining frontal collimated light and perfectly diffuse lights in different proportions according to Eq. (38) (ratio b from 0 to 1 in steps of 0.2). In every case, the irradiance on the horizontal plane is $E_z = \pi$, and the panel is still observed frontally, according to the z-axis.

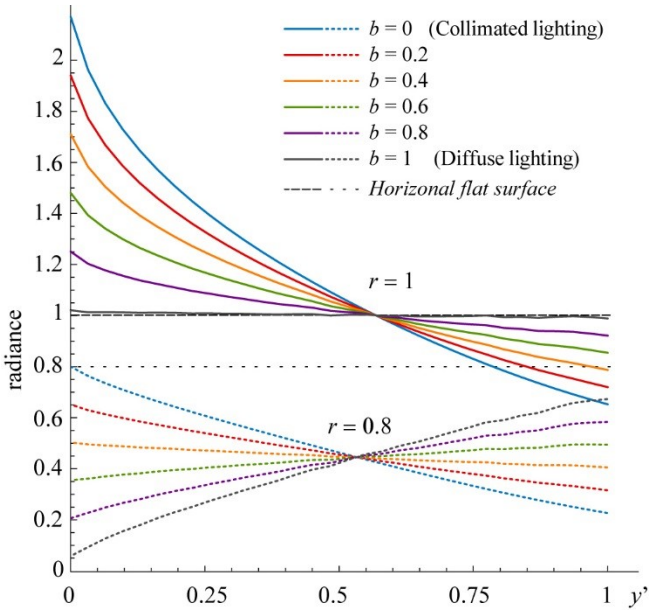

Figure 12 – Variation of the perceived radiance along the y'-axis on panel 1 in a V-cavity with angle α = 45° and reflectance r = 1 (solid lines) or 0.8 (dashed lines), for various illumination geometries obtained by mixing a fraction b of perfectly diffuse light and a fraction (1 – b) of frontal collimated light.

When illuminated by perflectly diffuse light, the perflectly non-absorbing cavity, with reflectance 1, displays a constant radiance equal to unity over the whole panel: it looks similar as a flat, horizontal surface made of the same material, which also displays a uniform radiance equal to unity. As soon as the illumination geometry contains a fraction of collimated light, the areas near the fold display a higher radiance and thus look brighter than the horizontal flat surface; in opposition, the areas near the external edge are darker than the horizontal flat surface. At a position on the panel around $y' = 0.6$, the radiance unity is displayed independently of the illumination geometry. For the material with reflectance $r = 0.8$, which is slightly absorbing, all points of the panel display a lower radiance than a horizontal flat surface of the same material, which would display a radiance 0.8. The areas near the fold are brighter than the ones near the external edge when the proportion of collimated light is high (low b values) but they look darker when the proportion of collimated light is low (high b values). As for the non-absorbing material, there is a position on the panel, around $y' = 0.55$, where the displayed radiance is independent on the illumination geometry.

Different variations as the ones displayed in Figure 12 would be obtained with other material reflectance values: the displayed radiance strongly decreases as the reflectance decreases. The cavity angle α, fixed to 45° in our simulations, also have a strong impact on the radiance gradient displayed by the cavity panels. A lower angle value strengthens both interreflection and shadowing effects, the first one tending to increase the displayed radiance near the fold, and the second one tending to decrease it. There is therefore a competition between the two phenomena, being generally in favor to the interreflection effect (brighter areas near the fold) under a rather collimated lighting, and in favor to the shadowing effect (brighter areas near the external edges) under a rather diffuse lighting.

The observation angle, not analyzed in this study, would also have an influence on the perceived radiance, especially at grazing angle where only the areas closest to external edge of one panel are observed, the other areas being masked by the other panel. Masking ca be treated by defining a similar Boolean function as for shadowing.

6. Conclusions

In this paper, we analyzed the interreflection effects occurring in concave surfaces under various illumination geometries, from collimated to perfectly diffuse lightings, through the simple case of V-cavities of infinite length made of a Lambertian material. Interreflections are known to increase the radiance exhibited by the concavities or the corners of the surface, but this stands mainly for a collimated illumination. In case of diffuse lighting, shadowing tends to decrease the irradiance of the surface in the concavities or corners, and therefore to make them darker than would be a flat surface of the same material. The reflectance of the material and the angle of the corner have also a strong impact on the competition between the interreflection effect and the shadowing effects, which can result in a higher radiance near the fold of the cavity than near its external edges, or in the opposite situation. An extension of the model presented here to V-cavities of finite-length would be interesting for practical applications, such as the creation of color charts with V-shaped color patches [17] whose potential to increase the accuracy of the color calibration of cameras has been recently shown by assuming collimated illumination. This model could help to see whether similar color calibration performance can be achieved when the illumination geometry contains diffuse light.

References

[1] R. H. Byrd, M. E. Hribar, and J. Nocedal, "An interior point algorithm for large-scale nonlinear programming," *SIAM Journal on Optimization* **9**, 877 (1999).
[2] M. Pharr, W. Jakob, and G. Humphreys, *Physically based rendering: From theory to implementation* (Morgan Kaufmann, 2016).
[3] H. W. Jensen, *Realistic image synthesis using photon mapping*, Ak Peters Natick, 2001.
[4] S. K. Nayar, K. Ikeuchi, and T. Kanade, "Shape from interreflections", *International Journal of Computer Vision* **6**, 173 (1991).
[5] S. K. Nayar and Y. Gong, "Colored interreflections and shape recovery," in *Image Understanding Workshop*, 333–343 (1992).
[6] S. M. Seitz, Y. Matsushita, and K. N. Kutulakos, "A theory of inverse light transport," *Tenth IEEE International Conference on Computer Vision, ICCV 2005*, vol. 2, 1440–1447 (2005).
[7] B. V. Funt and M. S. Drew, "Color space analysis of mutual illumination," *IEEE Transactions on Pattern Analysis and Machine Intelligence* **15**(12), 1319–1326 (1993).
[8] M. Liao, X. Huang, and R. Yang, "Interreflection removal for photometric stereo by using spectrum-dependent albedo," *IEEE Conference on Computer Vision and Pattern Recognition (CVPR)*, 689–696, (2011).
[9] Y. Fu, A. Lam, Y. Matsushita, I. Sato, and Y. Sato, "Interreflection removal using fluorescence," *European Conference on Computer Vision*, 203–217 (2014).
[10] M. S. Drew and B. V. Funt, "Calculating surface reflectance using a single-bounce model of mutual reflection," *IEEE Third International Conference on Computer Vision*, 394–399 (1990).
[11] J. Ho, B. V. Funt, and M. S. Drew, "Separating a color signal into illumination and surface reflectance components: Theory and applications," *IEEE Transactions on Pattern Analysis and Machine Intelligence* **12**(10), 966–977 (1990).

[12] J. J. Koenderink and A. Van Doorn, “Geometrical modes as a general method to treat diffuse interreflections in radiometry,” *J. Opt. Soc. Am.* **73**(6), 843–850 (1983).
[13] D. Forsyth and A. Zisserman, “Mutual illumination,” *IEEE Computer Society Conference on Computer Vision and Pattern Recognition (CVPR)*, 466– 473 (1989).
[14] D. Forsyth and A. Zisserman, “Shape from shading in the light of mutual illumination,” *Image and vision computing* **8**(1), 42–49 (1990).
[15] B. V. Funt, M. S. Drew, and J. Ho, “Color constancy from mutual reflection,” *International Journal of Computer Vision* **6**, 5–24 (1991).
[16] R. Deeb, D. Muselet, M. Hebert, A. Tremeau, J. van de Weijer, "3D color charts for camera spectral sensitivity estimation" BMVC 2017, London, 4-7 Sept. 2017.

Author Biography

Dorian Saint-Pierre received his engineering degree from the Institut d’Optique Graduate School, France (2016). He is now a Ph.D student at the University Jean Monnet of Saint-Etienne, France. His work is focused on material appearance modelling, and is co-sponsored by an industrial partner.